Estimation of Natural Gas Flaring Volume at the Western Siberia Flares using Satellite Night-Time Data in the Visible and Near-Infrared Range

Anatoly A. Lagutin, Egor Yu. Mordvin, Nikolay V. Volkov, Nina V. Tuchina

Altai State University, Barnaul, Russia

Abstract. The results of estimation of natural gas flaring volume at the Western Siberia flares for some periods of 2013-2019 are presented. These estimates were obtained in the framework of technology which includes the flares characteristic retrieval from satellite night-time data in the visible and near IR ranges, as well as the regression relationship between the source's power and the volume of the gas flaring. It was found that during this period the volume of gas flaring at the Western Siberia flares varied from 15.7 bcm in 2013 to 14.8 bcm in 2019.

Keywords: Western Siberia, gas flares, natural gas, flared gas volume, Suomi-NPP, VIIRS.

1 Introduction

Oil production at each field is accompanied by the emission of associated gas. A part of this gas is burned in flare units (FU) on oil production facilities, as well as at other stages of oil processing. According to the estimates of the National Oceanic and Atmospheric Administration, U. S. Department of Commerce, based on satellite observations, in 2015 there were 13,605 flare units in 88 countries [1]. Flared gas volume leaders are Russia, Iraq, Iran, Venezuela, and USA (see figure 2 of [1]). It is estimated [1] that about 140 billion cubic meters (bcm) of gas are flared annually in FU, which leads to the emission of about 300 million tons of CO_2.

It should be noted that, in addition to CO_2 and methane emissions, the associated gas flaring leads to atmospheric emission of nitric oxide, sulfur dioxide, soot and other toxic components, as well as to thermal effects on the underlying surface in the locations of the FU. These emissions influence climate, environment and human health at both the regional and global scales.

In the absence of regular and complete data on the locations of FUs and their operation mode, to estimate their impact on the Earth's biosphere it is necessary to monitor the characteristics of these units, as well as the "atmosphere – underlying surface" system in their locations. A key characteristic of this monitoring is the volume of associated gas flared.

Continuing research [1,2], the main goal of this work is to estimate the associated gas flaring volume at the Western Siberia flares using satellite night-time data in the visible and near-infrared range.

2 Informational base

The informational base of the study is the data from VIIRS (Visible Infrared Imaging Radiometer Suite) [3] onboard the Suomi-NPP satellite [4].

The 22 VIIRS spectral channels register electromagnetic radiation leaving the atmosphere in the 0.41–12.5 μm range. Unlike most devices of this class, 4 spectral channels of VIIRS detect the outgoing radiation flux in visible and near IR ranges at night-time. The characteristics of these channels are shown in table 1.

The scheme of processing of VIIRS/Suomi-NPP satellite information received in direct broadcast mode by the Altai State University ground stations consists of the following main steps:

- unpacking of satellite data;
- geolocation and calibration;
- cloud mask definition;
- search for thermal anomalies;
- determination of measured values (level 2 products).

Table 1. Specifications of VIIRS channels, detecting the outgoing radiation in the night-time in visible and near IR ranges.

Channel	Wavelength range (μm)	Sensitivity function maximum (μm)	Bandwidth (μm)	Pixel size (km×km)
DNB	0.500 – 0.900	0.700	0.400	0.742×0.742
M7	0.843– 0.881	0.862	0.042	0.742×0.776
M8	1.225 – 1.252	1.240	0.030	0.742×0.776
M10	1.571 – 1.631	1.601	0.060	0.742×0.776

3 Retrieval of FU parameters

The physical basis of the method for temperature retrieval of high-temperature thermal anomalies, including FUs, is the statement that on a moonless night, the entire flux of electromagnetic energy going into outer space in the visible and near infrared range, is basically the radiation of such source itself.

Registration of radiation in VIIRS channels in the visible and near IR ranges allows to retrieve the Planck distribution for the analyzed high-temperature source.

It is clear that the pixel that includes the anomaly is a gray body. In this case, the intensity recorded in this pixel by the VIIRS is equal to the product of the Planck function at the source temperature T and the scaling factor ε, which is defined as the ratio of the intensity observed by the satellite to the pixel intensity at this temperature T, provided that the entire pixel has this temperature [2]. The source area S is found by multiplying the pixel area by ε.

In the case of the flaring of pure methane, the combustion temperature of which is 2223 K, taking into account Wien's displacement law, it follows that the wavelength, which accounts for the maximum of intensity of radiation ~~is~~ equals to ~1.3 μm, i.e. it is between the channels M8 (1.2 μm) and M10 (1.6 μm) (see figure 1). This fact makes it possible to use the readings of the M10 channel as thresholds for the identification of thermal anomalies.

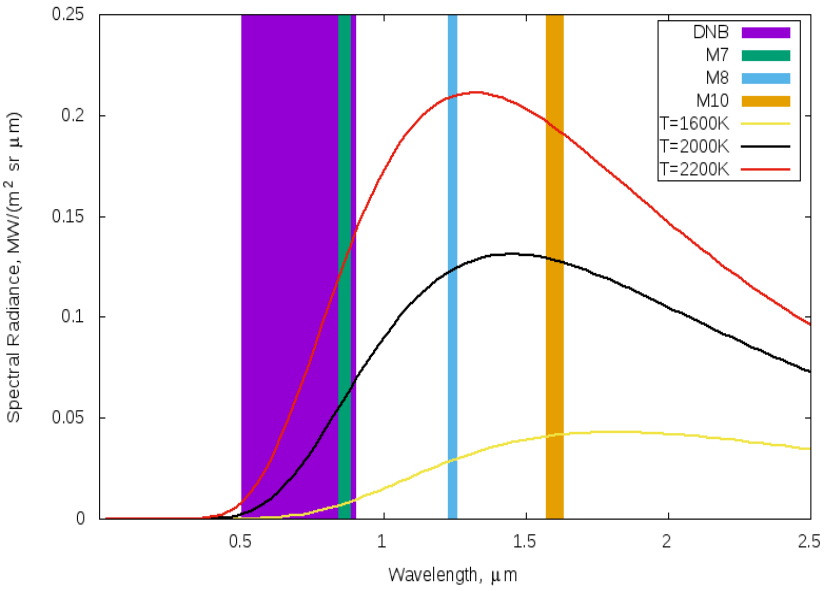

Figure 1. The Planck distribution at different temperatures of the source and the bandwidth of the VIIRS channels, recording the outgoing radiation in the night-time in the visible and near infrared ranges.

In the algorithm [5] used to determine the thermal anomalies, it is considered that such an anomaly is identified in a particular VIIRS pixel if the M10 channel reading for this pixel exceeds the threshold value $sr + 6std$, where sr is the average noise value in the M10 channel, and std is its standard deviation. For a scene pixel identified as a thermal anomaly, the source temperature T and scaling factor ε were retrieved. To solve this problem using the Levenberg-Marquardt algorithm, the optimization of the objective function of variables T and ε was carried out:

$$\min_{T,\varepsilon} F(T,\varepsilon) = \sum_{j=\{DNB,7,8,10,12,13\}} \left[L(\lambda_j) - \varepsilon B(T,\lambda_j)\right]^2. \quad (1)$$

In (1) the squares of residuals are summed for DNB, M7, M8, M10, M12 and M13 channels of the VIIRS radiometer. As initial values of the source temperature and the scaling factor $T_0 = 600$ K and $\varepsilon_0 = 0.01$ were used, respectively.

The source area was found using the expression $S = \Delta A \Delta D \varepsilon$ [5], where ΔA is the pixel size along the scanning direction, and ΔD – one along the satellite path (see expressions (4) and (5) of [5]).

4 High-temperature radiation sources in Western Siberia

The approach outlined above was implemented at the Space Monitoring Center of Altai State University to search for high-temperature sources of radiation from $T > 1500$ K in Western Siberia for 2013, 2015, 2017 and 2019. Thermal anomalies identified only once in a series of observations were excluded from further analysis.

As a result of the work for each of the study periods ~300 anomalies were found. As an example, figure 2 shows the spatial distribution of the sources found for 2013.

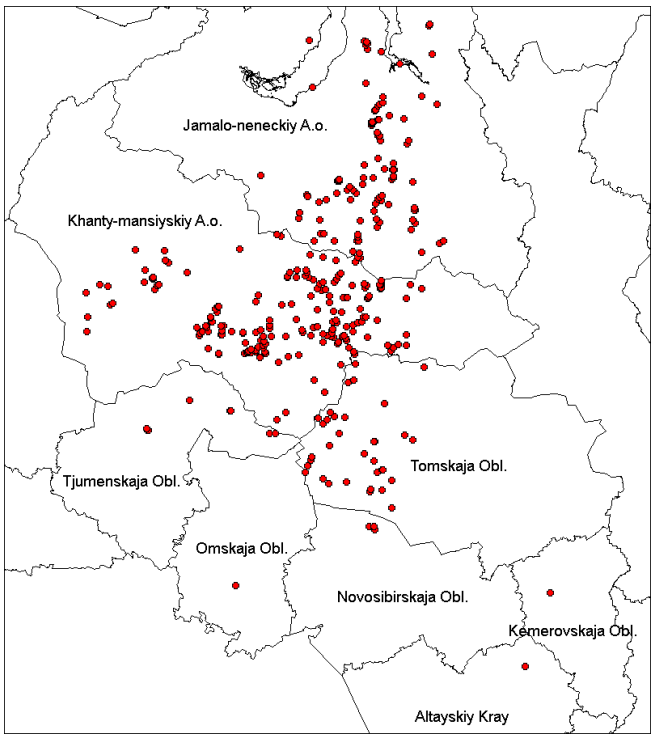

Figure 2. Spatial distribution of high-temperature thermal anomalies in Western Siberia, found for 2013.

The study of temperature variations of the found sources showed that for all investigated periods the values of T fall into the range of 1500–2300 K. This result indicate that these sources have an anthropogenic origin, and the range of the obtained temperatures indicates the combustion of the gas mixture on the basis of light hydrocarbons.

For visual identification/classification of sources, freely available geospatial data of Google Earth [6], Yandex.Maps [7], as well as high spatial resolution satellite imagery data from Landsat-8 [8] were used. Pooled analysis of these data showed that most of the sources found are flare units for natural gas flaring.

5 Estimation of the volume of flared gas

The estimation of the flared gas volume is based on the regression relationship between the source power measured by satellite device and the volume of the flared gas. This relationship is established in [2] according to the emissions from FUs of 47 countries. This ratio has the form

$$V = 0.0274 \cdot W, \tag{2}$$

where V is the volume of flared gas (in bcm), and W is the power of the source (in MW). The power of a source was obtained using the Stefan-Boltzmann law

$$W = \sigma T^4 S. \tag{3}$$

In [2] it was shown that there is a nonlinear relationship between W and the volume of flared gas V. This nonlinearity can be taken into account by the introduction of an exponent of source area in source power W assessment [2]

$$W = \sigma T^4 S^{0.7}. \quad (4)$$

Using the expressions (2) and (4) and the results of identification of high-temperature radiation sources, the volume of flared gas for each FU in Western Siberia was estimated. Total estimates of the volume of gas flared in the FUs of the region are presented in table 2.

Table 2. The estimation results of the volume of gas flared in the FUs of Western Siberia.

Year	Number of sources found	V, bcm
2013	336	15.7
2015	315	14.1
2017	291	14.9
2019	311	14.8

The obtained results show that the maximum volume of flared associated gas in the FUs of Western Siberia according to VIIRS data is observed in 2013 and equals to 15.7 bcm.

6 Conclusion

The results of estimation of natural gas flaring volume at the Western Siberia flares for 2013, 2015, 2017 and 2019 are presented. These estimates were obtained in the framework of technology which includes the flares characteristic retrieval from VIIRS/Suomi-NPP night-time data in the visible and near IR ranges, as well as the regression relationship between the source's power and the volume of the gas flaring. It was found that during this period the volume of gas flaring at the Western Siberia flares varied from 15.7 bcm in 2013 to 14.8 bcm in 2019.

References

[1] Elvidge C.D., Bazilian M.D., Zhizhin M. et al. The potential role of natural gas flaring in meeting greenhouse gas mitigation targets // Energy Strategy Reviews. 2018. Vol. 20. Pp. 156-162.

[2] Elvidge C.D., Zhizhin M., Baugh K. et al. Methods for global survey of natural gas flaring Visible Infrared Imaging Radiometer Suite data // Energies. 2016. Vol. 9.

[3] Hillger D., Kopp T, Lee T. et al. First-light imagery from SUOMI NPP VIIRS // BAMS. 2013. Vol. 94. Pp. 1019-1029.

[4] Powell A.M., Jr., Weng F. Introduction to special section on Suomi National Polar-Orbiting Partnership satellite calibration, validation, and applications // J. Geophys. Res. Atmos. 2013. Vol. 118. Pp. 12216–12217.

[5] Elvidge C.D., Zhizhin M., Hsu F-C. et al. VIIRS Nightfire: Satellite pyrometry at night // Remote Sens. 2013. Vol. 5. Pp. 4423-4449.

[6] Google Earth. https://www.google.com/earth/

[7] Yandex.Maps. https://yandex.ru/maps/

[8] USGS Earth Explorer. https://earthexplorer.usgs.gov/